Dramatic Enhancement of the Emission Current Density from Carbon Nanotube Based Nanosize Tips with Extremely Low Onset Fields

Kiran Shankar Hazra, Padmnabh Rai, Dipti Ranjan Mohapatra, Neha Kulshrestha, Reeti Bajpai, Soumyendu Roy, and D. S. Misra*

Department of Physics, Indian Institute of Technology Bombay, Mumbai-400 076, India

ABSTRACT Nanostructures based on multiwalled carbon nanotubes (MWNTs) are fabricated using plasma of the mixture of hydrogen and nitrogen gases. The plasma-sharpened tips of nanotubes contain only a few tubes at the apex of the structure and lead to the dramatic enhancement in the emission current density by a factor $>10^6$ with the onset field as low as 0.16 V/μm. We propose that the nature of the tunneling barrier changes significantly for a nanosize tip at very high local electric field and may lead to the saturation in the emission current density.

KEYWORDS: carbon nanotube · onset field · field emission · plasma-sharpened tip · square hill potential barrier

The field emission from the sharp tips with lower electrostatic fields has been satisfactorily explained in terms of the formulation given by Fowler and Nordheim (F−N) for the electrons tunneling through a triangular potential barrier present at the metal vacuum interface.[1−3] The F−N plots are routinely generated by measuring the current density from an electron-emitting surface as a function of electric field. Using F−N plots, one can determine the barrier height or the field enhancement factor for the electric field at the tips. However, for very high electrostatic field ($>10^9$ V/m), the phenomena of the electron emission remain unexplored, due to the practical difficulty of achieving such high electric fields. The reduction of the emitter tip size to low dimensions (of the order of a few nanometers) can enhance the electric field at the tip apex due to the heavily convergent electric lines of force on it. The carbon nanotubes (CNTs) would be an excellent candidate for studying the behavior of emitting tips at large electrostatic fields due to their extraordinary properties such as low dimensionality, high aspect ratio, high electrical conductivity, better current stability, longer lifetime, and lower turn on voltage.[4−8] Barring very few exceptions,[4,9−13] most of the groups working on field emission from CNTs have used the oriented samples, which are in the shape of a CNT forest grown perpendicular to the substrates.

We demonstrate a very novel and simple technique to sharpen the CNT pillars by using the plasma of a mixture of H_2 and N_2 at 600 °C to achieve the desired sharp conical tips with very few CNTs at the apex to give rise to very large electric field at the vicinity of the CNT tip.[14] At such high fields, these tips exhibit the field emission, which demonstrates the constancy of emission current at very low threshold voltage and a saturation region which can be explained by the tunneling of the electrons through a square hill potential barrier of constant value (V_0). Here we have shown that, as we decrease the tip diameter to the nanometer size, the triangular potential barrier converges into a square hill potential barrier, which leads to a very interesting saturation region in the $I-V$ plots of the CNT emitters explained in terms of the emission from a constant barrier.

RESULTS AND DISCUSSION

Figure 1a−f shows the SEM images of CNT pillar's structure after plasma sharpening for 15−55 s. Figure 1a shows the as-grown CNT pillar with forest shape morphology aligned perpendicular to the substrate. Figure 1b−f shows the variations in structure of CNT pillars as a function of the plasma sharpening time. The diameter and the height of the as-grown CNT pillars were ∼100 and ∼150 μm,

*Address correspondence to drk1955@gmail.com.

Received for review June 25, 2009 and accepted August 24, 2009.

Published online August 31, 2009.
10.1021/nn900674e CCC: $40.75

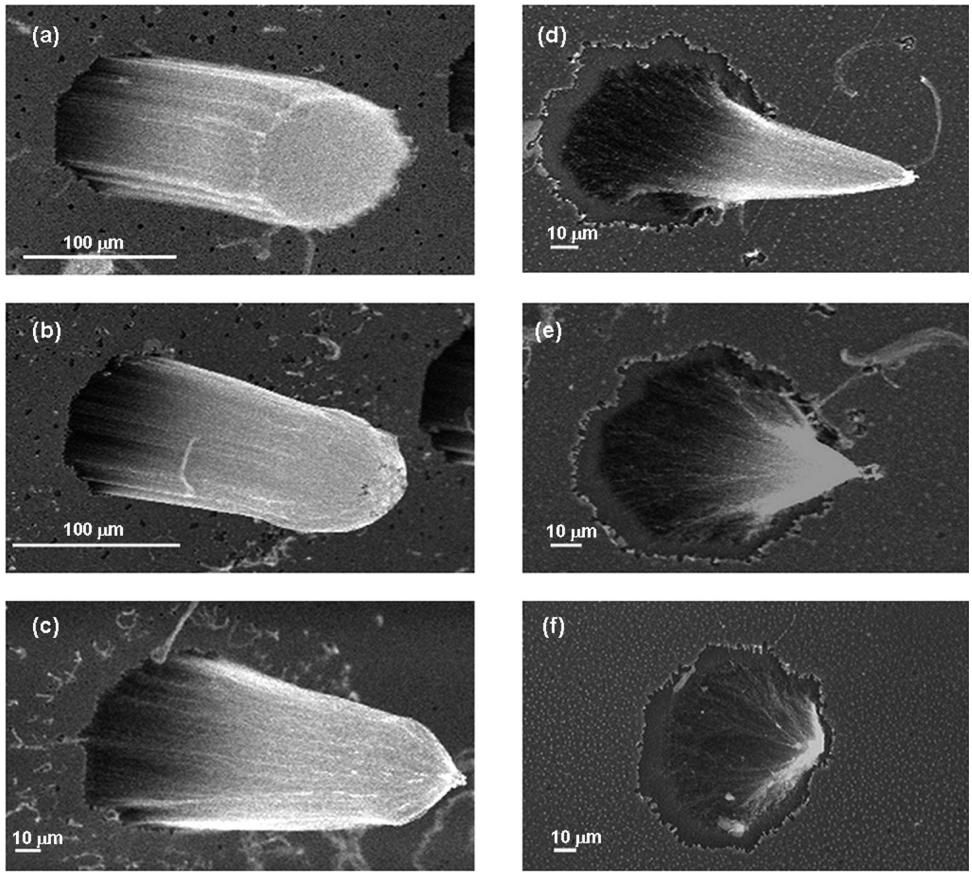

Figure 1. SEM micrograph of (a) as-grown CNT pillar and (b−f) after H_2 + N_2 plasma treatment for 15, 25, 35, 45, and 55 s.

respectively, before plasma etching. The morphology of the pillar changes dramatically with the plasma treatment; the height and the pillar tip diameter change significantly with different duration of plasma treatment (Table 1). The image of the samples after the plasma treatment for 15 and 25 s are shown in Figure 1b,c; the etching has taken place, but the conical tips are not yet sharply defined. The SEM image of the sample, plasma sharpened for 35 s, shows most interesting tip structure (Figure 1d) having an extremely sharp tip with long length so that the aspect ratio is very high. In this image, one can clearly see a few strands of CNTs sticking out at the apex of the sample. The images for the samples treated for 45 and 55 s, respectively, show that the over etching has been done and the sharpness of the tip is lost. The sharpest tip measured by SEM for Figure 1d is of the order of a few hundred nanometers, yet it is likely that it could be much smaller. Figure 2a,b shows the HRTEM images at lower and higher magnifications, respectively. It is evident that the CNTs forming the pillars are multiwalled in nature, and the walls of the CNTs are relatively devoid of defects. The typical diameter of the CNTs ranges from 25 to 45 nm, which supports the fact that there will be a very few MWNTs sticking out of the nanotip shown in Figure 1d. We believe that the tips of the CNTs are sharpened owing to the plasma treatment contributing to the dramatic enhancement in the emission currents.

In Figure 3, we have shown the field emission characteristics for the as-grown CNT pillars and the plasma-sharpened tips array on a log scale. For low electric fields, the current was observed to follow the Fowler−Nordeim law, where the current density J is related to applied electric field E as $J = A(\beta^2E^2/\phi)\exp(-B\phi^{3/2}/\beta E)$, with J in A/cm^2, $A = 1.56 \times 10^{-6}$ A V^{-2} eV, and $B = 6.83 \times 10^7$ eV$^{-3/2}$ V cm^{-1}; β is a field enhancement factor, ϕ is work function (eV), E is applied electric field in V/μm. The emission from the tip size of different diameters as well as lengths scales (Figure 1a−f) varies quite systematically, as shown in Figure 3a−f. The emission from the untreated pillars and for the plasma-sharpened tips for 55 s shows similar results (Figure 3a,f; at 0.40 V/μm applied field, the currents are 16 and 35 μA/cm^2, respectively), whereas the emission from the plasma-sharpened tip for 15 and 25 s demarks (Figure 3b,c) from untreated pillars dramatically (the enhancement in current density is on the order of 10^4). The plasma-sharpened tip for 35 s shows the most dramatic emission; the enhancement in current density from the pillars to the plasma-sharpened tips of 35 s

TABLE 1. Summary of Field Emission and SEM Analysis of the As-Grown as well as the Plasma-Sharpened CNT Pillar Array

plasma treatment time	length (μm)	tip diameter (μm)	base diameter (μm)	turn on voltage (V_{th}) (V/μm)	knee point for saturation current (V_s) (V/μm)	field enhancement factor (β) at low field region
0	150	100	100	0.36	0.44	5960
15	150	24	100	0.23	0.38	12600
25	144	5	92	0.22	0.32	14200
35	132	<1	80	0.16	0.23	16600
45	90	3	75	0.21	0.33	10380
55	65	12	75	0.35	0.48	5740

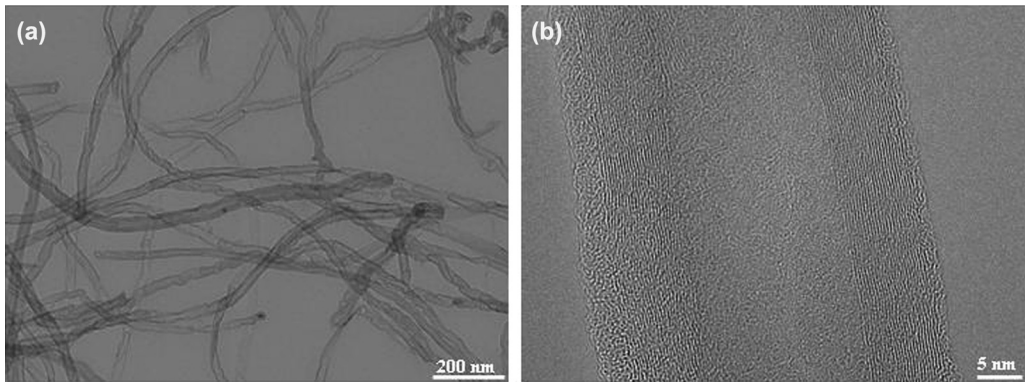

Figure 2. HRTEM images of (a) the CNTs at lower magnification and (b) for a single CNT at very high magnification.

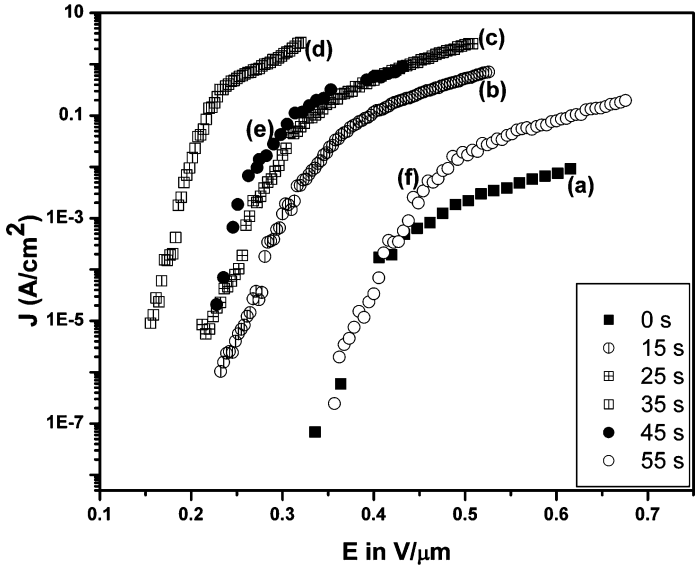

Figure 3. Field emission current density (in log scale) *versus* electric field (in log scale) for a vertically aligned CNT pillar array of (a) untreated sample and (b−f) after H_2 + N_2 plasma treatment for 15, 25, 35, 45, and 55 s.

is of the order $>10^6$, and the onset of the electric field for emission is remarkably low (≅0.16 V/μm with corresponding current density ≅10 μA/cm^2). In general, the onset fields for our samples are much smaller compared to the work reported by other groups on pillars and similar structures;[15−20] in particular, the onset field of 0.16 V/μm is the lowest reported in CNT samples. The F−N plots for all of the samples are plotted in Figure 4; in all of the curves, it is evident that the saturation in the current density is approaching at higher fields in conformity with Figure 3. Table 1 gives the summary of the emission results obtained on our samples.

The scaling of current densities as we change the tip size to nanometer dimensions appears to play a significant role in enhancing the field emission of the CNT pillars. The apex of the plasma-sharpened tip for 35 s may have only very few nanotubes contributing to the electronic emission current densities as the multiwalled CNTs may align with the application of high electric field,[21,22] and for such small dimensions, the values of current densities achieved (∼1.5 A/cm^2 at the applied field of 0.30 V/μm) in our case are remarkable.

Also, Figure 4 exhibits the nature of saturation in the sample with few nanotubes emitting electrons at the apex, showing the saturation of a very different nature than that shown by other samples and reported by other groups. In other samples, where the plasma-sharpened tip is still not of perfect shape (aspect ratio), the saturation is just approaching and the value of onset fields is larger (>0.21 V/μm). Predominantly, the space charge effects, adsorbates present on the samples, and contact resistance have been cited as the cause of saturation in the F−N plots.[23−26] However, as the apex becomes smaller and smaller of truly nanometer dimensions, the local electric field may become extremely large, leading to the alteration of the barrier significantly and change in the nature of the emission current.

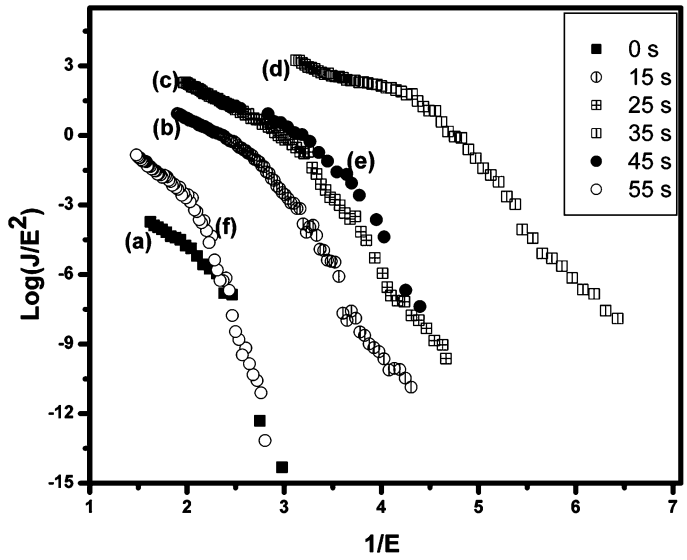

Figure 4. F−N plots for a vertically aligned CNT pillar array of (a) untreated sample and (b−f) after H_2 + N_2 plasma treatment for 15, 25, 35, 45, and 55 s.

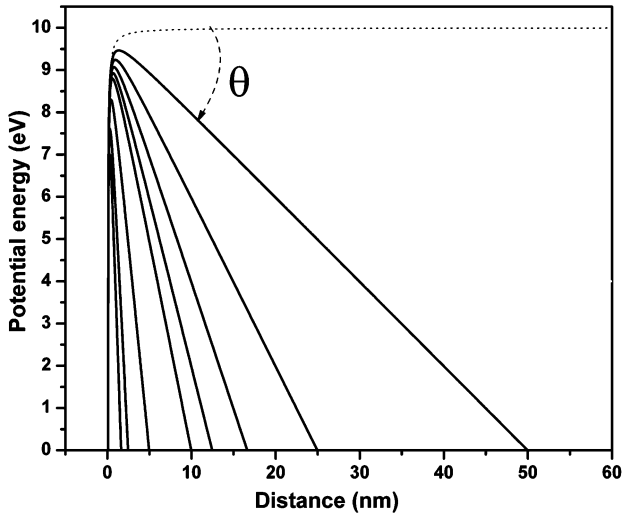

Figure 5. Continuous lines show the nature of potential barrier at the emitter surface for electric field varying from 2 × 10^8 to 10 × 10^8 V/m and then from 2 × 10^9 to 6 × 10^9 V/m (starting from the top) with the interval of 2 × 10^8 and 2 × 10^9 V/m, respectively. Dotted line is for the potential barrier without any applied field.

In Figure 5, we have plotted the CNT−vacuum electrostatic potential energy for various applied electric fields in the high field region, from 2 × 10^8 to 6 × 10^9 V/m. As given in the F−N model, we have used the same form of the potential at the CNT−vacuum interface, which is given by

$$V(x) = E_F + \phi - qxF - \frac{q^2}{16\pi\varepsilon_0 x} \qquad (1)$$

where q is the electronic charge; x is the normal distance coordinate to the CNT surface; E_F is the Fermi energy (~5.08 eV); ϕ is the work function (~5 eV); qxF is the potential energy due to external electric field; $q^2/16\pi\varepsilon_0 x$ is the potential energy due to the image charge. Figure 5 clearly shows that, with increase in the applied electric field, the tip apex−vacuum barrier bends down, resulting in the decrease of barrier height (V_0) as well as the barrier width. It can be noticed that the barrier bending is faster for lower field region (2 × 10^8 to 10 × 10^8 V/m) rather than the high field region (2 × 10^9 to 6 × 10^9 V/m), and after a certain high field, the barrier width becomes almost constant. In Figure 6, the barrier bending angle (θ) has been plotted against the electric field. The angle θ has been obtained from the slope of eq 1. For $x > x_0$, where $x_0 = 1/4\sqrt{(e/\pi\varepsilon_0 F)}$ (which is the normal distance coordinate to the emitter surface for maximum barrier height), the slope of the image term can be neglected and the effective slope of the tunneling barrier can be approximated to $-qF$.[2] The figure shows that up to 2 × 10^9 V/m (corresponding θ ~ 70°), θ changes rapidly following the linear dependence with electric field. Then it deviates from linear dependence, and θ starts varying very slowly with electric field. After the electric field reaches 6 × 10^9 V/m (corresponding θ ~ 80°), the variation of θ with electric field can be assumed as almost negligible. This allows us to approximate the tip apex−vacuum potential barrier as a square hill potential barrier of constant height $V_0 = E_F + \varphi$ and with very thin width (*i.e.*, L, which is of the order of a few angstroms). From Table 1, if we calculate the actual applied field at the knee point by multiplying β to the knee voltage (V_s) for the sharpest tip (Figure 1d), consisting of very few CNTs, we get the local electric field ~3.8 × 10^9 V/m, which matches closely with the knee point of the barrier bending angle (θ) *versus* electric field plot (Figure 6). This implies that the agreement between the theoretical estimate and the experimental value of the field at the apex of the sharpest tip is quite good. Thus, supporting our experimental condition for high electric fields, the form of the potential barrier can be approximated as

$$V(x) = E_F + \phi = V_0 \qquad (2)$$

Using this constant potential barrier, V_0, which is independent of x due to the potential bending nearly 90° at high electric field, we have formulated the saturation current density by following the conventional calculation reviewed by Good and Muller.[3] For the constant potential barrier, the probability for barrier penetration, $T(E)$, of the electron in the normal direction to the emitting surface with energy E can be rewritten after WKB approximation as

$$T(E) = \exp\left(-\left(\frac{8m}{\hbar^2}(V_0 - E)\right)^{1/2} L\right)$$

The supply function $N(E)dE$, which is the number of electrons moving along the x-direction with their energy within the range of E to $E + dE$, incident on the surface per unit area and time, is given by[3]

$$N(E)dE = \frac{4\pi m}{h^3}(E_F - E) \quad \text{when } E < E_F$$
$$= 0 \quad \text{when } E > E_F$$

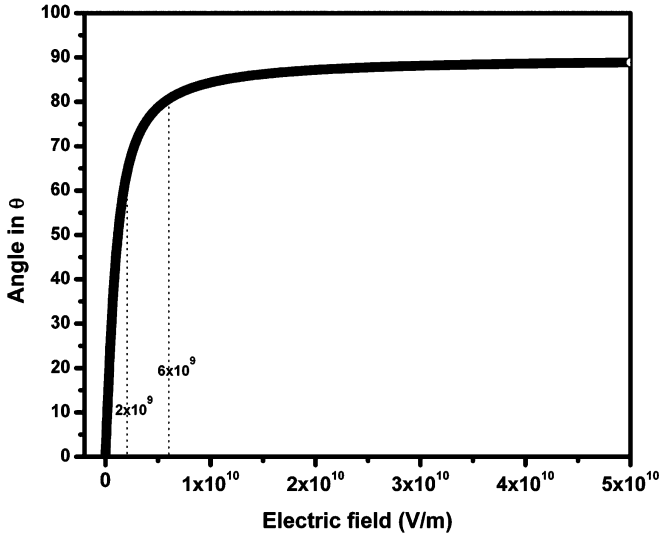

Figure 6. Barrier bending angle θ (as shown in Figure 5) *vs* applied electric field plot.

By Taylor series expansion around E_F and only keeping the first term of the integration, we get current density from the truly nanometer dimension tips as

$$J = J_0 \exp(-a\varphi^{1/2})E_F^2/2, \text{ where } J_0 = \frac{4\pi mq}{h^3} \text{ and } a = L\sqrt{\frac{8m}{\hbar^2}} \quad (3)$$

The above equation gives the current density for saturation region in very high electric field ($>2 \times 10^9$ V/m) and depends on work function (φ), barrier height (V_0), and the barrier width (L). For high field, the barrier width remains almost constant but the height of the barrier decreases by a factor of $\Delta\varphi = [1/2\sqrt{(\pi\varepsilon_0)}](e^3F)^{1/2}$, known as Schottky lowering.[2] For a large change in electric field, $\sim 2 \times 10^8$ V/m, $\Delta\varphi$ is $\sim$0.5 eV; that is, φ changes very slowly with electric field. Thus eq 3 can be taken as a slowly varying function of electric field, which explains the saturation in emission current, which is almost field independent. Thus, as the tip becomes sharper and sharper, the local electric field on each CNT apex increases and the emission current approaches the saturation region. Due to lower screening effect for the sharpest tip, a very high local electric field is applied on a few CNTs at the pillar tip apex, and it causes the required electric field to collapse the CNT vacuum barrier to a constant square hill potential barrier to achieve proper saturation current of CNTs.

CONCLUSION

In conclusion, a novel way of producing the plasma-sharpened nanotips based on carbon nanotube structures has been reported here. We find that the enhancement in the emission current density from the tip of nanosize is of the order of $>10^6$ with lowest onset field ($\sim$0.16 V/μm) reported so far in CNT samples. In the case of a perfect plasma-sharpened nanotip, the highly enhanced local electric field ($\geq 6 \times 10^9$ V/m) alters the triangular tunneling barrier to a constant square hill potential barrier that leads to the saturation of the emission current.

METHODS

CNT Growth. CNT pillars were synthesized by thermal chemical vapor deposition (CVD) technique on a patterned silicon wafer. The SiO_2 layer of 50 nm thickness was grown on a p-type (100) silicon wafer after RCA cleaning followed by wet oxidation. The patterns with a circular cross section of 100 μm diameter on the SiO_2 layer were fabricated by lift-off photolithography in a matrix of chrome−gold (Cr/Au) of 60 nm thickness. The Cr/Au layer is used to avoid the growth of CNTs on locations other than the circular silicon oxide patterns. The column and row separation of 250 μm was kept to prevent the CNT pillars from overlapping onto one another. A liquid mixture of toluene/ferrocene was evaporated and transported into the hot zone of the tube furnace by hydrogen gas flow of $\sim$70 sccm. The synthesis time for CNTs was 45 min, and the deposition temperature was kept at $\sim$850 $\pm$ 10 °C. The mixture of floating catalyst ferrocene and toluene yields the growth of vertically aligned CNTs in the pillar shape.

Plasma Treatment. The plasma treatment of as-grown CNT pillar array was carried out in a mixture of hydrogen and nitrogen ($H_2 + N_2$) plasma generated by microwave power. The flow rates of H_2 and N_2 gases of 6 N purity were 40 and 10 sccm, respectively. The optimized operating temperature and pressure for the plasma treatment were 600 °C and 10 Torr, respectively. Plasma treatment was carried out for a series of samples for a range of time period $\cong$15−55 s.

Instrumentation. The morphological changes of CNT pillar array samples were imaged by JEOL model JSM-6400 scanning electron microscope (SEM). High-resolution TEM measurements have been carried out using a 200 keV JEOL UHR machine. The field emission characteristics of the sample before and after plasma sharpening for different time were measured in a high vacuum chamber with a parallel diode-type configuration, at the base pressure of $\sim 5 \times 10^{-7}$ mbar. The anode−cathode distance was adjusted by a micrometer screw, controlled from the outside of the chamber. The field emission current was measured at different voltages using an automatically controlled Keithley 6514 electrometer and SRS power supply (model PS-325).

Acknowledgment. We deeply acknowledge Prof. V. R. Rao and the Microelectronics Group of Electrical Eng. Department, IIT Bombay, for the lithography and SEM facility.

REFERENCES AND NOTES

1. Fowler, R. H.; Nordheim, L. Electron Emission in Intense Electric Fields. *Proc. R. Soc. London, Ser. A* **1928**, *119*, 173–181.
2. Nordheim, L. W. The Effect of the Image Force on the Emission and Reflexion of Electrons by Metals. *Proc. R. Soc. London, Ser. A* **1928**, *121*, 626–639.
3. Good, R. H., Miiller, E. W., Eds. *Hundbueh der Physik*; Springer-Verlag: Berlin, 1956; pp 176−191.
4. Rinzler, A. G.; Hafner, J. H.; Nikolaev, P.; Lou, L.; Kim, S. G.; Tomanec, D.; Nordlander, P.; Colbert, D. T.; Smalley, R. E. Unraveling Nanotubes: Field Emission from an Atomic Wire. *Science* **1995**, *269*, 1550–1553.
5. De Heer, W. A.; Châtelain, A.; Ugarte, D. A A Carbon Nanotube Field-Emission Electron Source. *Science* **1995**, *270*, 1179–1180.
6. Wang, Q. H.; Corrigan, T. D.; Dai, J. Y.; Chang, R. P. H.; Krauss, A. R. Field Emission from Nanotube Bundle Emitters at Low Fields. *Appl. Phys. Lett.* **1997**, *70*, 3308–3310.
7. Rao, A. M.; Jacques, D.; Haddon, R. C.; Zhu, W.; Bower, C.; Jin, S. *In Situ*-Grown Carbon Nanotube Array with Excellent Field Emission Characteristics. *Appl. Phys. Lett.* **2000**, *76*, 3813–3815.
8. Murakami, H.; Hirakawa, M.; Tanaka, C.; Yamakawa, H. Field Emission from Well-Aligned, Patterned, Carbon Nanotube Emitters. *Appl. Phys. Lett.* **2000**, *76*, 1776–1778.
9. Saito, Y.; Hamaguchi, K.; Hata, K.; Uchida, K.; Tasaka, Y.; Ikazaki, F.; Yumura, M.; Kasuya, A.; Nishina, Y. Conical Beams from Open Nanotubes. *Nature* **1997**, *389*, 554–555.
10. Bonard, J. M.; Dean, K. A.; Coll, B. F.; Klinke, C. Field Emission of Individual Carbon Nanotubes in the Scanning Electron Microscope. *Phys. Rev. Lett.* **2002**, *89*, 197602-1–197602-4.
11. Minoux, E.; Groening, O.; Teo, K. B. K.; Dalal, S. H.; Gangloff, L.; Schnell, J. P.; Hudanski, L.; Bu, I. Y. Y.; Vincent, P.; Legagneux, P.; Amaratunga, G. A. J.; Milne, W. I. Achieving High-Current Carbon Nanotube Emitters. *Nano Lett.* **2005**, *5*, 2135–2138.
12. Teo, K. B. K.; Chhowalla, M.; Amaratunga, G. A. J.; Milne, W. I.; Pirio, G.; Legagneux, P.; Wyczisk, F.; Pribat, D.; Hasko,

D. G. Field Emission from Dense, Sparse, and Patterned Arrays of Carbon Nanofibers. *Appl. Phys. Lett.* **2002**, *80*, 2011–2013.
13. Smith, R. C.; Cox, D. C.; Silva, S. R. P. Electron Field Emission from a Single Carbon Nanotube: Effects of Anode Location. *Appl. Phys. Lett.* **2005**, *87*, 103112-1–103112-3.
14. Rai, P.; Mohapatra, D. R.; Hazra, K. S.; Misra, D. S.; Tiwari, S. P. Nanotip Formation on a Carbon Nanotube Pillar Array for Field Emission Application. *Appl. Phys. Lett.* **2008**, *93*, 131921-1–131921-3.
15. Fan, S.; Chapline, M. G.; Franklin, N. R.; Tombler, T. W.; Cassell, A. M.; Dai, H. Self-Oriented Regular Arrays of Carbon Nanotubes and Their Field Emission Properties. *Science* **1999**, *283*, 512–514.
16. Bonard, J. M.; Weiss, N.; Kind, H.; Stöckli, T.; Forró, L.; Kern, K.; Châtelain, A. Tuning the Field Emission Properties of Patterned Carbon Nanotube Films. *Adv. Mater.* **2001**, *13*, 184–188.
17. Fujii, S.; Honda, S.; Machida, H.; Kawai, H.; Ishida, K.; Katayama, M.; Furuta, H.; Hirao, T.; Oura, K. Efficient Field Emission from an Individual Aligned Carbon Nanotube Bundle Enhanced by Edge Effect. *Appl. Phys. Lett.* **2007**, *90*, 153108-1–153108-3.
18. Weng, T. W.; Lai, Y. H.; Lee, K. Y. Area Effect of Patterned Carbon Nanotube Bundle on Field Electron Emission Characteristics. *Appl. Surf. Sci.* **2008**, *254*, 7755–7758.
19. Killian, J. L.; Zuckerman, N. B.; Niemann, D. L.; Ribaya, B. P.; Rahman, M.; Espinosa, R.; Meyyappan, M.; Nguyen, C. V. Field Emission Properties of Carbon Nanotube Pillar Arrays. *J. Appl. Phys.* **2008**, *103*, 064312-1–064312-7.
20. Seelaboyina, R.; Boddepalli, S.; Noh, K.; Jeon, M.; Choi, W. Enhanced Field Emission from Aligned Multistage Carbon Nanotube Emitter Arrays. *Nanotechnology* **2008**, *19*, 065605-1–065605-4.
21. Wei, Y.; Xie, C.; Dean, K. A.; Coll, B. F. Stability of Carbon Nanotubes under Electric Field Studied by Scanning Electron Microscopy. *Appl. Phys. Lett.* **2001**, *79*, 4527–4529.
22. Einarsson, E.; Tuggle, D. W.; Jiao, J. *In-Situ* Alignment Of Carbon Nanocoils and Their Field Emission Behavior Induced by an Electric Field. *Appl. Phys. A: Mater. Sci. Process.* **2004**, *79*, 2049–2054.
23. Chen, Y.; Deng, S. Z.; Xu, N. S.; Chen, J.; Ma, X. C.; Wang, E. G. Physical Origin of Non-Linearity in Fowler−Nordheim Plots of Aligned Large Area Multi-Walled Nitrogen-Containing Carbon Nanotubes. *Mater. Sci. Eng., A* **2002**, *327*, 16–19.
24. Deana, K. A.; Chalamala, B. R. Current Saturation Mechanisms in Carbon Nanotube Field Emitters. *Appl. Phys. Lett.* **2000**, *76*, 375–377.
25. Fransen, M. J.; van Rooy, T. L.; Kruit, P. Field Emission Energy Distributions from Individual Multiwalled Carbon Nanotubes. *Appl. Surf. Sci.* **1999**, *146*, 312–327.
26. Zhang, J.; Yang, C.; Yang, W.; Feng, T.; Wang, X.; Liu, X. Appearance of a Knee on the Fowler−Nordheim Plot of Carbon Nanotubes on a Substrate. *Solid State Commun.* **2006**, *138*, 13–16.